Nature. Author manuscript; available in PMC 2016 July 04.

Published in final edited form as:

Nature. 2013 February 07; 494(7435): 60–64. doi:10.1038/nature11783.

Structural basis for viral 5′-PPP-RNA recognition by human IFIT proteins

Yazan M. Abbas[1], **Andreas Pichlmair**[2,3,*], **Maria W. Górna**[2,*], **Giulio Superti-Furga**[2], and **Bhushan Nagar**[1]

[1]Department of Biochemistry and Groupe de Recherche Axe sur la Structure des Proteines McGill University, Montreal, QC H3G 0B1, Canada

[2]CeMM Research Center for Molecular Medicine of the Austrian Academy of Sciences, Vienna, Austria

[3]Max Planck Institute of Biochemistry, Martinsried, Germany

Abstract

IFIT proteins are interferon-inducible, innate immune effector molecules that are thought to confer antiviral defence through disruption of protein-protein interactions in the host translation initiation machinery. However, recently it was discovered that IFITs could directly recognize viral RNA bearing a 5′-triphosphate group (PPP-RNA), which is a molecular signature that distinguishes it from host RNA. Here, we report crystal structures of human IFIT5, its complex with PPP-RNAs, and an N-terminal fragment of IFIT1. The structures reveal a new helical domain that houses a positively charged cavity designed to specifically engage only single stranded PPP-RNA, thus distinguishing it from the canonical cytosolic sensor of double stranded viral PPP-RNA, RIG-I. Mutational analysis, proteolysis and gel-shift assays reveal that PPP-RNA is bound in a non-sequence specific manner and requires approximately a 3-nucleotide 5′-overhang. Abrogation of PPP-RNA binding in IFIT1 and IFIT5 were found to cause a defect in the anti-viral response by HEK cells. These results demonstrate the mechanism by which IFIT proteins selectively recognize viral RNA and lend insight into their downstream effector function.

Correspondence and request for materials should be addressed to B.N. (bhushan.nagar@mcgill.ca) or G.S.-F. (gsuperti@cemm.oeaw.ac.at).

*These authors contributed equally to this work

Supplementary Information accompanies the paper on www.nature.com/nature.

Author Contributions: B.N., G.S.-F., Y.M.A., M.W.G. and A.P. designed the project. B.N., Y.M.A, A.P., M.W.G. and G.S.-F wrote the manuscript. Y.M.A. performed all of the structural and biochemical analysis, and carried out proteolysis and gel-shift experiments. M.W.G. performed the mutagenesis, pulldown, and gel-shift experiments and A.P. performed functional experiments and pulldown experiments.

Competing interests statement: The authors declare that they have no competing financial interests.

Coordinates and structure factors have been deposited in the Protein Data Bank under accession codes 4HOQ, 4HOR, 4HOS, 4HOT and 4HOU.

Keywords

innate immunity; TPR; IFIT1; ISG56; interferon; viral RNA; triphophosphate RNA; IFIT5; ISG58; crystal structure

The innate immune system relies on several germ-line encoded receptors to distinguish self from non-self molecules in order to mount an appropriate early defence response. During viral infection, non-self molecules are derived from viral genomes generally in the form of double-stranded RNA (dsRNA) or 5′-triphosphorylated RNA (PPP-RNA) that is not protected by a 5′-cap. The canonical host proteins responsible for sensing or interacting with these foreign nucleic acids include the Toll-like receptors (TLRs), retinoic acid-inducible gene I (RIG-I)-like receptors (RLRs) and nucleotide oligomerization domain (NOD)-like receptors (NLRs)[1]. Recently, an unbiased proteomics approach discovered that the interferon-induced proteins with tetratricopeptide repeats (IFITs) could also directly engage PPP-RNA[2].

IFITs are among the most potently expressed proteins of a group of interferon-stimulated genes (ISGs)[3], which are the culmination of virally triggered signalling pathways that lead to the production of interferon α/β and other cytokines. They are evolutionarily conserved from mammals to fish, of which in humans there are four well-characterized paralogues, IFIT1 (p56/*ISG56*), IFIT2 (p54/*ISG54*), IFIT3 (p60/*ISG60*) and IFIT5 (p58/*ISG58*), ranging in mass from 54 to 56 kDa. IFITs are composed of tetratricopeptide repeats (TPRs), which are a degenerate, 34-amino acid, helix-turn-helix motif usually present in multiple copies as tandem arrays that generate solenoid-type scaffolds well suited for mediating protein-protein interactions[4] (Supplementary Figs. 1 and 2).

IFITs have been implicated in modulating several biological processes including inhibition of translation initiation, cell proliferation, and migration; as well as mediating antiviral effects[3]. Most of these functions are thought to occur through disruptive protein-protein interactions between IFITs and host cellular factors. Through their TPRs, human IFIT1 and IFIT2 were shown to inhibit key steps during translation initiation by interacting with the ‘e’ or ‘c’ subunits of eIF3[5,6]. However, the surprising finding that IFITs can bind RNA suggested a more direct role – following infection/interferon-stimulation, it was found that IFITs form large multi-protein complexes with other family members and several different RNA binding proteins, leading to viral clearance[2]. Like RIG-I, productive binding of both IFIT1 and IFIT5 were shown to depend on the presence of cytosolic PPP-RNAs[2,7,8]. However, crystallographic and biochemical analyses of RIG-I bound to RNA revealed that it is a dsRNA-specific translocase[9], which optimally interacts with blunt ended PPP-RNA[10–15]. The mechanism by which IFITs recognize PPP-RNA is unknown.

We describe here the crystal structure of full-length human IFIT5 with and without PPP-RNAs, as well as an N-terminal, protease-resistant fragment of human IFIT1 (nIFIT1). The structures reveal a novel arrangement of TPR domains that directly bind PPP-RNA in a non-sequence specific manner and, to our knowledge, represent the first example of a TPR-protein bound to a nucleic acid ligand. Structure guided biochemical analysis of IFIT5 indicated that only single stranded RNA (ssRNA) can be accommodated within the protein,

which undergoes a compaction upon binding. Finally, functional analysis in human embryonic kidney (HEK) cells reveals a reduction of viral replication only in the presence of proper PPP-RNA binding by IFIT1 or IFIT5.

Crystal structures of IFIT5 and nIFIT1

We crystallized and determined the structures of full-length human IFIT5 (residues 1–482) at 2.1Å resolution and an N-terminal fragment of IFIT1 (residues 7–279) at 1.9Å resolution using single-wavelength anomalous diffraction (SAD). The structure of IFIT5 reveals a helical domain with approximate dimensions of 80Å × 55Å × 40Å (Fig. 1a and 1b). In most multi-TPR-containing proteins such as O-linked GlcNAc transferase (OGT), the relationship between successive TPRs is regular and repeating such that they form open-ended superhelical structures with distinct convex and concave surfaces[4,16]. In IFIT5, of its total 24 α-helices, 18 form canonical TPRs (TPRs 1–9; Fig. 1a), while the remaining 6 helices intervene between the TPRs such that the regular repeating relationship between them is disrupted. This results in the formation of three distinct bundles of TPRs (Subdomains I, II and III) oriented with respect to one another to give the overall protein a relatively closed clamp-shaped structure (Fig. 1a and Supplementary Fig. 5a).

The topology of Subdomain I is unusual in that its two canonical TPRs (α3 to α6) are capped off on both ends by helices α1 and α2, preventing its further propagation into a superhelix. This is facilitated by a connecting 17-residue loop (L1) containing a highly conserved CHFTW pentapeptide motif that is invariant among the overwhelming majority of IFIT proteins (Supplementary Fig. 2), and forms a single turn of a helix that packs against the concave inner face of Subdomain I (Supplementary Fig. 4). This same arrangement of Subdomain I is also found in the structure of nIFIT1 (r.m.s.d. 1.4 Å; Supplementary Fig. 3) and is likely a defining characteristic of all IFIT proteins given the high TPR and sequence conservation in Subdomains I and II (Supplementary Fig. 1 and 2).

The remainder of the IFIT5 structure forms a superhelix encompassing Subdomains II and III, as well as a pair of extended non-TPR helices (α15 and α16) that form a pivot point between the latter two subdomains (Fig. 1b). Subdomain II forms a canonical four-TPR repeat domain where strikingly, its first helix (α7) interacts with Subdomain I in a manner reminiscent of TPR protein-ligand interactions observed previously[17] (Supplementary Fig. 4). This leads to the concave surface of Subdomain II forming one wall of a large cavity in the centre of the protein closed off at its base by helix a2 (Fig. 1b). The same TPR-ligand relationship between Subdomains I and II is maintained in the nIFIT1 structure as well (Supplementary Fig. 3).

The rest of the cylindrical cavity is created by the intervening pivot helices and the N-terminal TPRs from Subdomain III. Subdomain III begins with two typical TPRs followed by an interrupting helix (α21), which inverts the direction of the final TPR9 such that it forms an S-shaped appendage at the C-terminus with two potential ligand-interacting concave surfaces (Fig. 1b and Supplementary Fig. 5b). The deep pocket formed by this atypical arrangement of TPRs is approximately 28Å deep by 15Å wide, and is lined with an

expansive collection of positively charged residues well suited for the accommodation of nucleic acid (Fig. 1c).

IFIT5 specifically binds PPP-RNAs

To understand the structural basis for RNA binding by IFIT5, we *in vitro* transcribed 5′-triphosphate-bearing, short oligonucleotides of cytidine, uridine, and adenosine, purified each PPP-RNA in complex with IFIT5 (Supplementary Fig. 6), and determined their structures at resolutions of 1.86Å (oligo-C), 2.0 Å (oligo-U) and 2.5 Å (oligo-A) using molecular replacement with the apo-structure. All of the structures were similar, therefore we initially describe the general features of IFIT5-oligo-C complex since it was the highest resolution structure. Difference Fourier maps revealed strong positive electron density within the central positively charged pocket from which the 5′-triphosphate and the first four nucleotides of the RNA could be reliably modelled (Fig. 2a and Supplementary Fig. 10a). The 5′-triphosphate group is nestled deep within the pocket and makes a multitude of electrostatic interactions with protein side chains from helix α2 (Glu33, Thr37 and Gln41) located at the very base of the pocket, and residues from the concave inner surface of Subdomain II (Lys150, Tyr250 and Arg253) (Fig. 2c). Arg186, which in IFIT1 (Arg187) was previously identified to be required for RNA interaction, makes a weak salt-bridge with the α– and β-phosphates and Van der Waal contacts with the first ribose moiety. These RNA interacting residues are for the most part conserved in sequence and structure between IFIT5 and IFIT1 (Supplementary Figs. 2 and 7), the only IFITs that have been shown to bind PPP-RNA with significant affinity[2]. One notable exception is Thr37, which is replaced in IFIT1 by Arg38, suggesting slight differences in RNA recognition between IFIT1 and IFIT5. Conversely in IFIT3, which is known to not bind PPP-RNA[2], Tyr250 is substituted with a negatively charged residue – Asp242, and Arg186 with His182 (Supplementary Fig. 2), both of which would directly interfere with RNA binding.

Interestingly, a metal ion that bridges the α- and γ-phosphates also appears to be an integral part of PPP-RNA recognition as it neutralizes the negative charge in this region from Glu33 (Fig. 2c and Supplementary Fig. 8). Based on ligand distances and geometry, the ion is likely Mg^{2+} from the *in vitro* transcription reactions, but could potentially also be Na^{+} (a component of the crystallization buffer). It is unlikely that capped mRNA can be accommodated within this pocket owing to size constraints. Additionally, given the critical interactions made with the γ-phosphate and the metal ion, the pocket is unlikely to accept with significant affinity 5′-monophosphorylated or 5′-hydroxylated RNA. Thus, the structure of the IFIT5 TPR domains have evolved to specifically engage PPP-RNA, and in doing so, distinguish between self and non-self nucleic acids.

Following the 5′-triphosphate end of the RNA, the first two nucleotides (N1, N2) are stably bound along the pocket before the third and fourth nucleotides (N3, N4) begin to protrude from the mouth of the pocket (Fig. 2b). Well-defined density is observed for the phosphodiester backbone and ribose sugars (Supplementary Fig. 10a), which also form several specific interactions with the protein (Fig. 2c). In particular, the 5′-phosphate of N2 hydrogen bonds with Tyr254 and that of N3 makes a salt-bridge with Arg260 and Lys257, and hydrogen bonds with Gln288 (Fig. 2c). The 5′-phosphate of N4 interacts with Arg294,

and weak electron density was observed for the 5′-phosphate of a fifth nucleotide (Supplementary Fig. 11a). The 2′-hydroxyl of the ribose sugars also make specific interactions with the protein, but in this case, interactions that are dependent on the sugar pucker. N1 adopts a C2′-endo conformation (commonly found in B-form dsDNA, Supplementary Fig. 9) and hydrogen bonds with Tyr156 (Fig. 2c), whereas N2 and N3 are C3′-endo (as found in A-form dsRNA) and interact via their 2′-hydroxyls with His287/Gln288 and Arg294/Asp343, respectively (Fig. 2c and Supplementary Fig. 11a).

PPP-RNA recognition is non-sequence specific

To investigate the potential for sequence specific interactions at the 5′-end, we compared the crystal structures of IFIT5 in complex with the different RNAs. In both the oligo-C and oligo-U complexes, the pyrimidine base at position 1 is abutted from the top by Van der Waal interactions with Tyr156 and two glycine residues from the loop of TPR3 (between α7 and α8), and from the bottom by non-specific stacking interactions against the second base, which in turn stacks with Phe337 (Fig. 2c). Notably, the first two bases do not make any specific hydrogen bonds with protein residues and there is ample space adjacent to the pyrimidine ring edges, suggesting that the larger purine bases can also be easily accommodated (Fig. 3). The structure of the oligo-A complex confirms this notion and reveals that the adenine rings reach further out into the periphery making additional non-specific Van der Waals contacts with Thr371, His374 and Phe339, which were absent with the pyrimidine bases (Fig. 3b–d).

The remaining bases stack against Phe339 in a manner analogous to that observed for the first two bases (Fig. 2b right and Supplementary Fig. 11) and interact with a mobile loop from TPR4. Thus, IFIT5 appears to have evolved the capacity to accommodate any 5′-PPP-RNA sequence that may potentially be present in a viral genome.

PPP-RNA binding involves a conformational change

Because the RNA binding site in IFIT5 is a deep and narrow pocket, the means by which RNA enters is unclear. Superposition of the RNA-bound and free forms of IFIT5 reveal that the RNA-bound state is more compact, with the largest motions occurring at the pivot helices between Subdomain III and the rest of the protein (Fig. 4a and Supplementary Fig. 13). These motions position several key residues from the different subdomains for optimal interaction with the RNA. Moreover, limited proteolysis of IFIT5 in the presence and absence of RNA supports the notion of compaction and stabilization of the protein in the RNA-bound form (Fig. 4b and Supplementary Fig. 15).

To better understand the nature of the conformational change upon RNA binding, we employed small-angle X-ray scattering (SAXS) measurements, which provide information on macromolecular size, state and flexibility directly in solution[18,19]. SAXS analysis revealed significant reductions in the radius of gyration (R_g, ~2.5 Å), the maximum dimension ($D_{max,}$ ~25 Å) and the volume (~14000 $Å^3$) of the protein upon addition of RNA (Fig. 4c and Supplementary Fig. 14). The scattering curves show good agreement between solution (R_g, 28.2 Å) and crystal structure (R_g, 27.5 Å) for the RNA-bound form

(Supplementary Fig. 14h), in contrast to the apo form, which displays significant differences (solution R_g, 30.6 Å; crystal structure R_g, 28.3 Å). This suggests that in solution, the apo-protein is either more open or possibly flexible. To discern between these possibilities, we subjected the SAXS data to a Porod-Debye analysis, which provides information on the degree of flexibility present in the scattering sample[19]. For both apo and RNA-bound IFIT5, the Porod-Debye plot showed characteristic plateaus that indicate the presence of distinct conformations for both species (Supplementary Fig. 14k,l). Thus, apo-IFIT5 likely exists in a more open conformation in solution than that observed in the crystal structure, facilitating RNA entry.

IFIT5 and IFIT1 bind only single stranded PPP-RNAs

The internal diameter of the RNA binding pocket in IFIT5 is roughly 15 Å, leaving no room to accommodate dsRNA, which would require a diameter of greater than 21 Å. Moreover, at least three bases are necessary to span the length of the pocket suggesting that IFIT5 is potentially a sensor for PPP-ssRNA, or base-paired PPP-RNA with a minimum three-nucleotide overhang. By contrast, foreign PPP-RNA species in the cytosol that optimally activate RIG-I appear to require blunt-ended RNAs, which are thought to be the most potent immune-stimulant of RIG-I[15].

To assess the recognition of distinct PPP-RNA species by IFITs, we employed gel shift assays. A 44-nucleotide ssRNA with no predicted secondary structure within the 5′-22 nucleotides was *in vitro* transcribed to which complementary RNA strands of 15 – 20 nucleotides were annealed to generate dsRNA with blunt ends and various 5′-overhangs. Consistent with the crystal structure, we found that IFIT5 could shift both PPP-ssRNA and PPP-dsRNA with at least 3-nucleotide overhangs, but could not efficiently shift blunt-ended PPP-RNA or PPP-dsRNA with 1–2 nucleotide overhangs (Fig. 5a and Supplementary Fig. 16). Similarly, IFIT1 could only shift PPP-ssRNA or PPP-dsRNA with at least 5-nucleotide overhangs (Supplementary Fig. 16). As a negative control we used IFIT3, and it could not shift any species of RNA (Fig. 5a and Supplementary Fig. 16b). Thus, owing to the limitations imposed by their RNA binding pockets, IFIT5 and IFIT1 can engage only PPP-RNAs that have single-stranded 5′-ends.

Functional validation of PPP-RNA binding to IFITs

To examine the functional significance of residues involved in binding PPP-RNA, we used PPP-RNA coated beads to pull down myc-tagged wild-type and mutant IFIT5 and IFIT1 expressed in HEK293 cells. We began by first corroborating that IFIT5, like IFIT1, could be pulled down by RNA only when it is triphosphorylated at the 5′-end (Supplementary Fig. 17a) and replacing the triphosphate with 5′-cap, 5′-monophosphate or 5′-OH diminishes the binding significantly (Fig. 5b). The affinity of PPP-RNA for IFIT5 is between 250–500 nM (Fig. 5b), similar to that found previously for IFIT1[2].

Next, we mutated key RNA contacts within the pocket and found that in most cases, a single residue substitution was sufficient to abolish RNA binding *in vitro* (Fig. 5c). All residues recognizing the PPP-RNA were critical for binding, with the exception of Glu33, Y156 and

H287 (see Supplementary Fig. 17). Homologous mutations in IFIT1 also lead to abrogation of RNA binding. Thus, the PPP-RNA binding pocket identified here is likely involved in a similar mode of recognition in other IFIT family members.

Finally, to investigate whether the RNA interacting residues are important for the antiviral activity of IFIT5 against virus infection, we used HEK293 Flp-In TREx-cells that inducibly express IFIT5, and IFIT5 mutants that have lost their ability to bind PPP-RNA. Consistent with the mutational analysis, IFIT5 mutants were impaired in their ability to restrict growth of vesicular stomatitis virus compared to wild-type IFIT5 (Fig 5d). Similarly, IFIT1 lacking the ability to bind PPP-RNA was not able to inhibit the activity of an influenza virus polymerase (Fig. 5e), consistent with the notion that binding to PPP-RNA is critical for the antiviral activity of IFIT1.

Discussion

The structural basis for IFIT recognition of foreign RNA described here validates the new paradigms put forth for how this family of ISGs carry out their effector functions, and brings to the forefront the versatility of the TPR motif in recognizing diverse ligands, paralleling established receptors of the innate immune system such as those containing leucine-rich repeats[1].

In addition to using protein-protein interactions to confer downstream anti-viral activity[2,3,5,6], the principal molecular role of IFITs appears to be initiated by direct recognition of foreign single stranded PPP-RNAs. PPP-RNAs are found within the genome of negative sense (−) ssRNA viruses such as influenza and vesicular stomatitis virus. Other RNA viruses, such as positive-sense (+) viruses which have 5′-capped genomes, can also generate cytosolic PPP-RNAs as replicative intermediates during their lifecycle. Hence, the evolution of a binding site to specifically recognize PPP-RNA allows IFITs to distinguish self from non-self RNAs since cytosolic host ssRNAs bear a 5′-monophosphate (on rRNA and tRNA)[20,21] or are 5′-capped (in the case of mRNA). In doing so, one possible mechanism for IFIT function may be to latch onto the ends of viral RNA preventing it from being properly replicated or packaged into progeny virions.

Recent studies have suggested a role for IFIT proteins in sensing the 5′-cap methylation status of some viral RNA (eg. West Nile virus, poxvirus and coronavirus)[22–24]. While a 5′-cap is present on (+) virus genomes, most viruses also have the ability to either hijack a cap from host mRNA or encode machinery to add a 5′-cap structure to their mRNA, thereby potentially circumventing IFIT recognition[25]. Although a 5′-cap cannot be accommodated within the RNA binding pocket of IFIT5 identified here, we do not preclude the possibility that higher order complexes of IFITs may be able to recognize capped viral RNAs.

Finally, given that bacterial mRNAs also bear a free 5′-PPP and can access the cytosol during infection to potentiate induction of interferon-β[26], it is plausible that IFITs could also play a role in anti-bacterial innate immunity. Taken together, it is clear that unravelling the structural details that underlie IFIT biology will improve our understanding of the complex

interplay between pathogens and host innate immunity, and hopefully pave the way for the development of new immunotherapeutics.

Methods Summary

For crystallization, all constructs were cloned into a modified pet28a vector containing an N-terminal, Ulp1-cleavable, 6xHis-SUMO tag[27] and expressed in *E. coli*. Proteins were purified using standard Ni-affinity, ion-exchange, and size-exclusion chromatography. PPP-RNAs were generated by *in vitro* transcription. Crystals of nIFIT1, IFIT5, and IFIT5 with PPP-RNA were grown from a sparse matrix screen (see online methods). The structures of nIFIT1 and IFIT5 were solved by SAD phasing of Seleno-Methionine derivatized protein, and the complexes with PPP-RNA were solved by molecular replacement using apo-IFIT5 as a search model. Pull-downs with PPP-RNA and functional assays with HEK Flp-in cells are described elsewhere[2]. Full methods can be found online in the Supplementary file.

Supplementary Material

Refer to Web version on PubMed Central for supplementary material.

Acknowledgments

We thank Shaun Labiuk and Pawel Grochulski for X-ray data collection performed on beamline 08ID-1 at the Canadian Light Source, which is supported by the Natural Sciences and Engineering Research Council of Canada, the National Research Council Canada, the Canadian Institutes of Health Research, the Province of Saskatchewan, Western Economic Diversification Canada, and the University of Saskatchewan. Thanks also to all lab members for helpful discussions and technical assistance. B.N. is supported by a Canada Research Chair, a Career Development Award from the Human Frontiers Science Program (CDA 0018/2006-C/1) and an operating grant from the Canadian Institutes of Health Research (CIHR grant MOP-82929). Work in the G.S.-F. laboratory is funded by the Austrian Academy of Sciences and the i-FIVE ERC grant. A.P. is an EMBO long-term fellowship recipient (ATLF 463-2008). Y.M.A. was supported by the CIHR Strategic Training Initiative in Chemical Biology.

References

1. Barbalat R, Ewald SE, Mouchess ML, Barton GM. Nucleic Acid Recognition by the Innate Immune System. Annu Rev Immunol. 2011; 29:185–214. [PubMed: 21219183]
2. Pichlmair A, et al. IFIT1 is an antiviral protein that recognizes 5′-triphosphate RNA. Nat Immunol. 2011; 12:624–630. [PubMed: 21642987]
3. Fensterl V, Sen GC. The ISG56/IFIT1Gene Family. J Interferon Cytokine Res. 2011; 31:71–78. [PubMed: 20950130]
4. Main ERG, Xiong Y, Cocco MJ, D'Andrea L, Regan L. Design of stable alpha-helical arrays from an idealized TPR motif. Structure. 2003; 11:497–508. [PubMed: 12737816]
5. Guo J, Hui DJ, Merrick WC, Sen GC. A new pathway of translational regulation mediated by eukaryotic initiation factor 3. EMBO J. 2000; 19:6891–6899. [PubMed: 11118224]
6. Terenzi F, Hui DJ, Merrick WC, Sen GC. Distinct induction patterns and functions of two closely related interferon-inducible human genes, ISG54 and ISG56. J Biol Chem. 2006; 281:34064–34071. [PubMed: 16973618]
7. Pichlmair A, et al. RIG-I-Mediated Antiviral Responses to Single-Stranded RNA Bearing 5′-Phosphates. Science. 2006; 314:997–1001. [PubMed: 17038589]
8. Hornung V, et al. 5′-Triphosphate RNA is the ligand for RIG-I. Science. 2006; 314:994–997. [PubMed: 17038590]
9. Myong S, et al. Cytosolic viral sensor RIG-I is a 5′-triphosphate-dependent translocase on double-stranded RNA. Science. 2009; 323:1070–1074. [PubMed: 19119185]

10. Wang Y, et al. Structural and functional insights into 5′-ppp RNA pattern recognition by the innate immune receptor RIG-I. Nat Struct Mol Biol. 2010; 17:781–787. [PubMed: 20581823]
11. Lu C, et al. The Structural Basis of 5′ Triphosphate Double-Stranded RNA Recognition by RIG-I C-Terminal Domain. Structure. 2010; 18:1032–1043. [PubMed: 20637642]
12. Kowalinski E, et al. Structural Basis for the Activation of Innate Immune Pattern-Recognition Receptor RIG-I by Viral RNA. Cell. 2011; 147:423–435. [PubMed: 22000019]
13. Luo D, et al. Structural Insights into RNA Recognition by RIG-I. Cell. 2011; 147:409–422. [PubMed: 22000018]
14. Jiang F, et al. Structural basis of RNA recognition and activation by innate immune receptor RIG-I. Nature. 2011; 479:423–427. [PubMed: 21947008]
15. Schlee M, et al. Recognition of 5′ triphosphate by RIG-I helicase requires short blunt double-stranded RNA as contained in panhandle of negative-strand virus. Immunity. 2009; 31:25–34. [PubMed: 19576794]
16. Jínek M, et al. The superhelical TPR-repeat domain of O-linked GlcNAc transferase exhibits structural similarities to importin alpha. Nat Struct Mol Biol. 2004; 11:1001–1007. [PubMed: 15361863]
17. Zhang Y, Chan DC. Structural basis for recruitment of mitochondrial fission complexes by Fis1. Proc Natl Acad Sci USA. 2007; 104:18526–18530. [PubMed: 17998537]
18. Putnam CD, Hammel M, Hura GL, Tainer JA. X-ray solution scattering (SAXS) combined with crystallography and computation: defining accurate macromolecular structures, conformations and assemblies in solution. Q Rev Biophys. 2007; 40:191–285. [PubMed: 18078545]
19. Rambo RP, Tainer JA. Characterizing flexible and intrinsically unstructured biological macromolecules by SAS using the Porod-Debye law. Biopolymers. 2011; 95:559–571. [PubMed: 21509745]
20. Xiao S, Scott F, Fierke CA, Engelke DR. Eukaryotic ribonuclease P: a plurality of ribonucleoprotein enzymes. Annu Rev Biochem. 2002; 71:165–189. [PubMed: 12045094]
21. Fromont-Racine M, Senger B, Saveanu C, Fasiolo F. Ribosome assembly in eukaryotes. Gene. 2003; 313:17–42. [PubMed: 12957375]
22. Daffis S, et al. 2′-O methylation of the viral mRNA cap evades host restriction by IFIT family members. Nature. 2010; 468:452–456. [PubMed: 21085181]
23. Züst R, et al. Ribose 2′-O-methylation provides a molecular signature for the distinction of self and non-self mRNA dependent on the RNA sensor Mda5. Nat Immunol. 2011; 12:137–143. [PubMed: 21217758]
24. Szretter KJ, et al. 2′-O methylation of the viral mRNA cap by West Nile virus evades ifit1-dependent and -independent mechanisms of host restriction in vivo. PLoS Pathog. 2012; 8:e1002698. [PubMed: 22589727]
25. Decroly E, Ferron F, Lescar J, Canard B. Conventional and unconventional mechanisms for capping viral mRNA. Nat Rev Microbiol. 2011; 10:51–65. [PubMed: 22138959]
26. Sander LE, et al. Detection of prokaryotic mRNA signifies microbial viability and promotes immunity. Nature. 2011; 474:385–389. [PubMed: 21602824]
27. Mossessova E, Lima CD. Ulp1-SUMO crystal structure and genetic analysis reveal conserved interactions and a regulatory element essential for cell growth in yeast. Mol Cell. 2000; 5:865–876. [PubMed: 10882122]

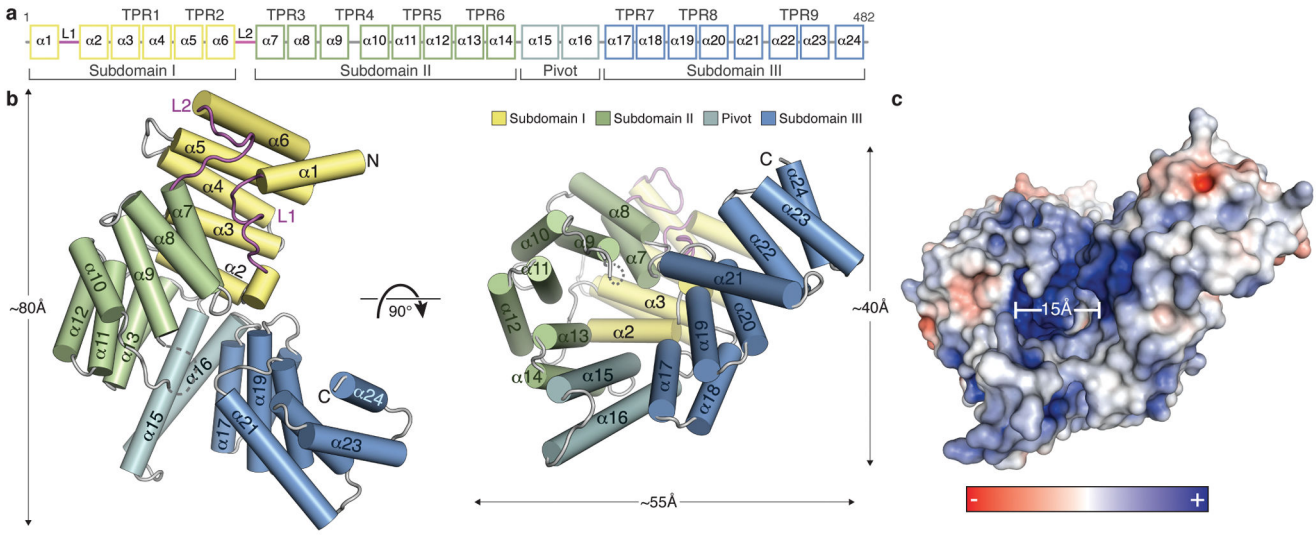

Figure 1.

Structural overview of human IFIT5. **a**, Secondary structure, TPR motif and subdomain organization of IFIT5. **b,** Orthogonal views of IFIT5 with helices represented as cylinders. **c,** Surface representation of IFIT5 coloured by electrostatic potential (using APBS) from $-5kTe^{-1}$ (red) to $+5kTe^{-1}$(blue).

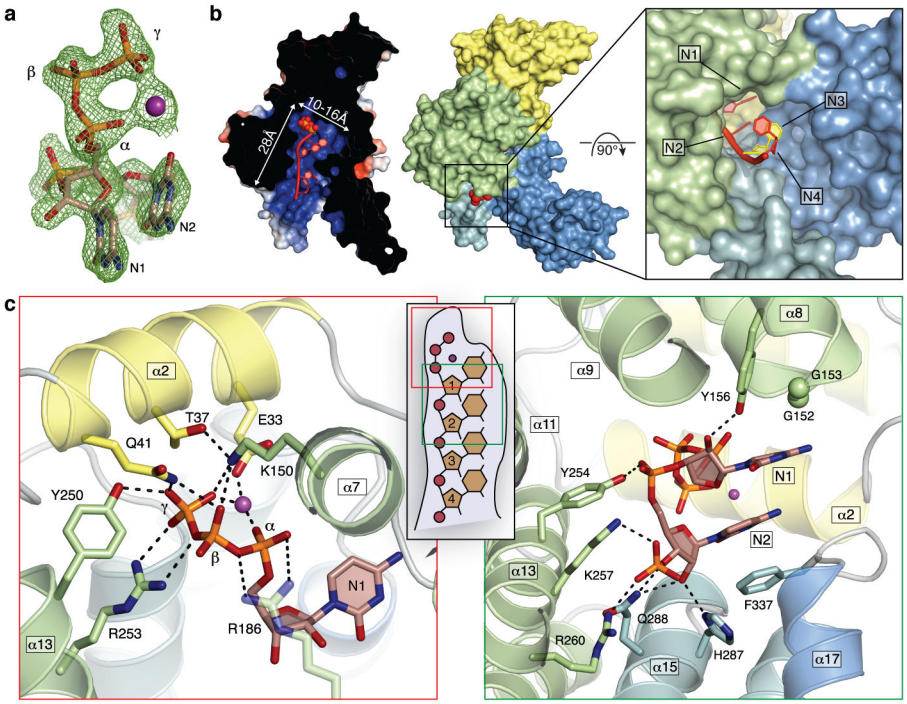

Figure 2.

Structure of IFIT5 bound to PPP-RNA. **a,** F_O-F_C electron density map of the triphosphate and first two nucleotides contoured at 3.5σ before inclusion of RNA into the model. The metal ion is indicated with a purple sphere. **b,** Left: cross-section of the complex coloured by surface electrostatic potential. The triphosphate is shown as spheres and RNA nucleotides are shown in red. Middle: surface representation of IFIT5 bound to PPP-RNA coloured by subdomain. Protruding RNA is shown as red spheres. Right: close-up view looking down the axis of the RNA binding pocket. **c,** Close-up view of the residues making specific contacts with the triphosphate group (left) and the first two nucleotides, N1 and N2 (right). Helices are coloured according to the subdomain to which they belong. Hydrogen bond/salt-bridge interactions are indicated with black dashed lines.

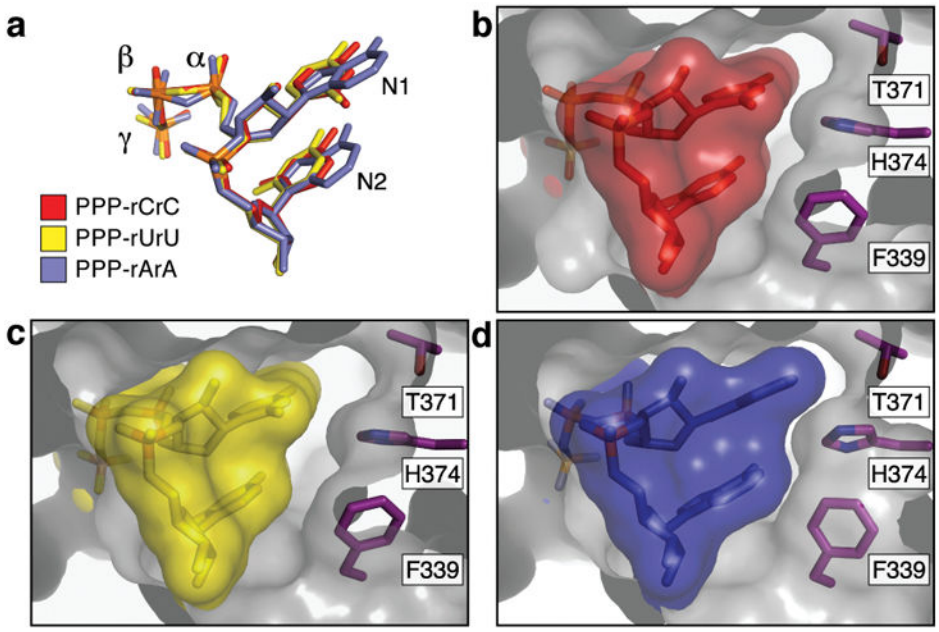

Figure 3.

The interaction between IFIT5 and PPP-RNA is non-sequence specific. Close up of the RNA binding pocket in an orientation similar to that of Fig. 2b, right panel. **a,** Alignment of the first two nucleotides from the three IFIT5-RNA complexes. **b, c,** Surface and stick representation of the first two nucleotides within the IFIT5-oligo-C and IFIT5-oligo-U complexes. The protein surface is depicted as a transparent grey cutaway. **d,** IFIT5-oligo-A complex. Detailed binding between the protein and all nucleotides is depicted in Supplementary Fig. 12.

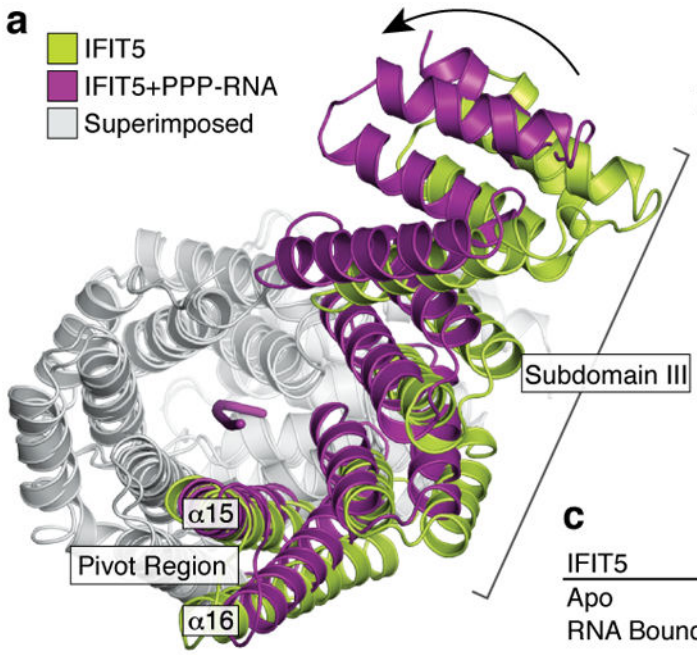

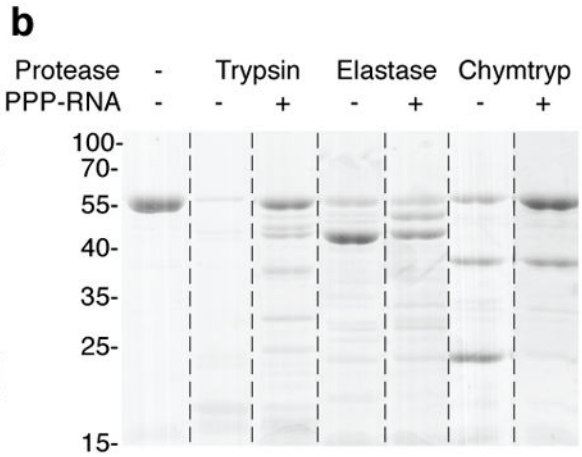

c

IFIT5	Solution R_g (Å)	Dmax (Å)	Volume (Å^3)
Apo	30.6 ± 0.32	120 ± 6.0	80526 ± 6871
RNA Bound	28.2 ± 0.53	93.3 ± 2.1	67283 ± 3027

Figure 4.

IFIT5 undergoes a conformational change upon binding PPP-RNA. **a,** Comparison of IFIT5 bound to PPP-RNA (magenta) and the unbound form (green). Superimposed regions are coloured light grey. **b,** SDS-PAGE gel of limited protease digestion of IFIT5 in the absence and presence of RNA taken from each experiment at the 15 min time point (see also Supplementary Fig. 15). **c,** Summary of SAXS results. Measurements are the average from 3 concentrations, with the corresponding standard deviation.

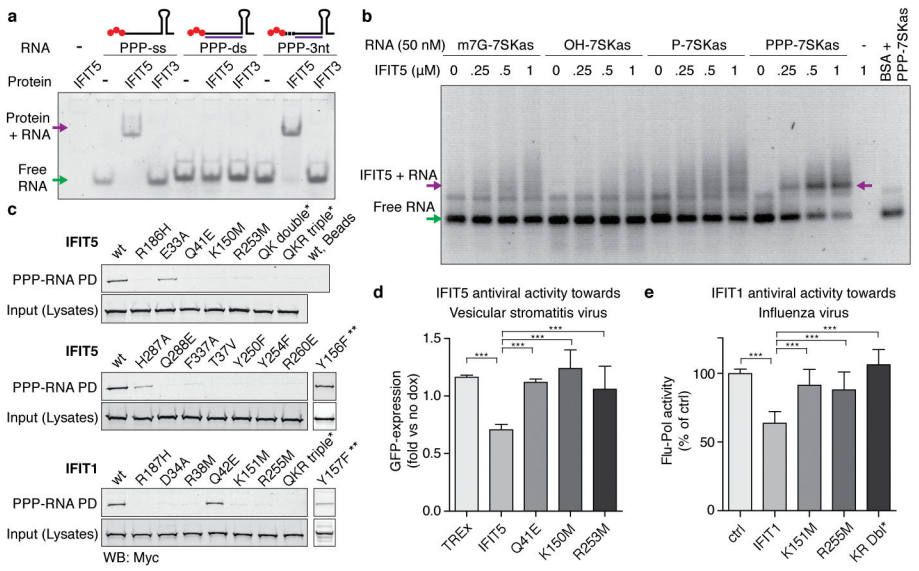

Figure 5.

Functional analyses of IFIT binding to PPP-RNA. **a**, Mobility shift assay between IFIT5/IFIT3 and ssRNA, dsRNA with blunt ends, or dsRNA with a 3-nucleotide overhang as indicated by the schematics above each set of lanes (PPP, red spheres; *in vitro* transcribed top strand, black line; synthetic complementary RNA, purple). **b,** Agarose gel shift assay between IFIT5 and various RNAs indicated. **c,** Biotinylated RNA pulldowns (PD) of wild-type (wt) and mutant IFIT1 and IFIT5 from HEK293 cell lysates. * QK Double is Q41E/K150M and QKR Triple is Q21E/K150M/R253M. ** Y156F and Y157F where carried out separately, and the appropriate positive and negative controls found in Supplementary Fig. 17. **d** and **e,** PPP-RNA binding is required for antiviral activities of IFIT5 and IFIT1. **d**, Replication of Vesicular stomatitis virus expressing GFP in doxycycline (dox) inducible HEK-Flp-In cells expressing IFIT5 (and mutants). Average fold change (+/− SD) in dox-treated versus untreated cells of ten measurements. **e**, Influenza virus in 293T cells transfected with IFIT1 (and mutants). Average percentage (+/− SD) of influenza polymerase activity as compared to control (ctrl) of four independent experiments done in duplicate measurements. *** = $p < 0.001$ (1 way ANOVA, Tukey's Multiple Comparison Test).